Diffusion measurement with transverse beam echoes

Yuan Shen Li, Carleton College
Mentor: Tanaji Sen, Fermilab

Abstract

Beam diffusion is an important measure of stability in high intensity beams. Traditional methods of diffusion characterization (e.g. beam scraping) can be very time-consuming. In this study, we investigated transverse beam echoes as a novel technique for measuring beam diffusion. With aid of both analytical and numerical solutions, we analyzed variations in maximum echo amplitude with and without diffusion. We performed a self-consistent measurement of diffusion coefficient D_1 via a parameter scan over delay time τ. We also demonstrated the effectiveness of pulsed quadrupoles as a means to boost echo amplitude. Results from this study will support the planned echo experiments in the IOTA proton ring under construction at Fermilab.

Lee Teng Fellowship in Accelerator Science and Engineering

1 Background

As part of the new "intensity frontier" in high energy physics, accelerator physicists are pushing the boundaries of attainable beam power. In particular, Fermilab is planning to upgrade its proton accelerator facility to provide multi-MW beam output [1], thus paving the way for discoveries in areas such as neutrino and muon physics.

A significant challenge to the reliable operation of high intensity beams is beam diffusion due to space charge and other intensity dependent effects. If left unchecked, these forces can cause beam emittance to grow dramatically over time. The first step in overcoming this would be a reliable method to characterize beam diffusion. However, the traditional method of diffusion characterization using beam scraping is a very time-intensive process that could take many hours to complete [2].

In this study, we investigate a novel method for diffusion measurement using transverse beam echoes. The echo is an intricate phenomenon arising from phase space dynamics and has been extensively studied in the form of plasma wave echoes in plasma physics and spin echoes in nuclear magnetic resonance (NMR). Transverse echoes in beam physics was first discussed in the 1990s [3]. The echo signal amplitude is extremely sensitive to any phase perturbation and thus soon became a promising candidate for probing diffusion. Perhaps more importantly, measuring the echo is a relatively quick affair, normally requiring only several thousand turns.

With the aid of computer simulation, we characterize the behavior of the transverse echo signal under linear diffusion and test pulsed quadrupole sequences as a means to boost echo amplitude. Finally, we aim to provide practical recommendations for the planned echo measurement experiment at the Integrable Optics Test Accelerator (IOTA) proton ring at Fermilab.

2 Theory

2.1 Basic echo sequence

Beam echoes have been observed in both transverse and longitudinal phase spaces [4]. In our study, we shall restrict our discussion to the transverse variety. Define the usual position coordinate x and momentum coordinate $p \equiv \beta x' + \alpha x$, where β, α are the Courant-Snyder parameters. It is also convenient to define the corresponding Floquet coordinates,

$$\xi \equiv \frac{x}{\sqrt{\beta}}, \qquad \eta \equiv \frac{p}{\sqrt{\beta}}. \tag{1}$$

Following usual convention, the action-angle variables are

$$J \equiv \frac{x^2 + p^2}{2\beta} = \frac{\xi^2 + \eta^2}{2}, \tag{2}$$

$$\tan\phi \equiv -\frac{p}{x} = -\frac{\eta}{\xi}. \tag{3}$$

In a linear lattice, the action J is conserved. Thus phase advance can be described by a simple rotation in Floquet phase space. However, upon adding nonlinear ring elements (e.g. octupoles) there will be an action-dependence in the betatron frequency $\omega = \omega(J)$, and J is no longer conserved. Particles with different J will experience different phase advance every turn, giving rise to phase decoherence. This is the first key ingredient of the transverse beam echo (Fig. 1).

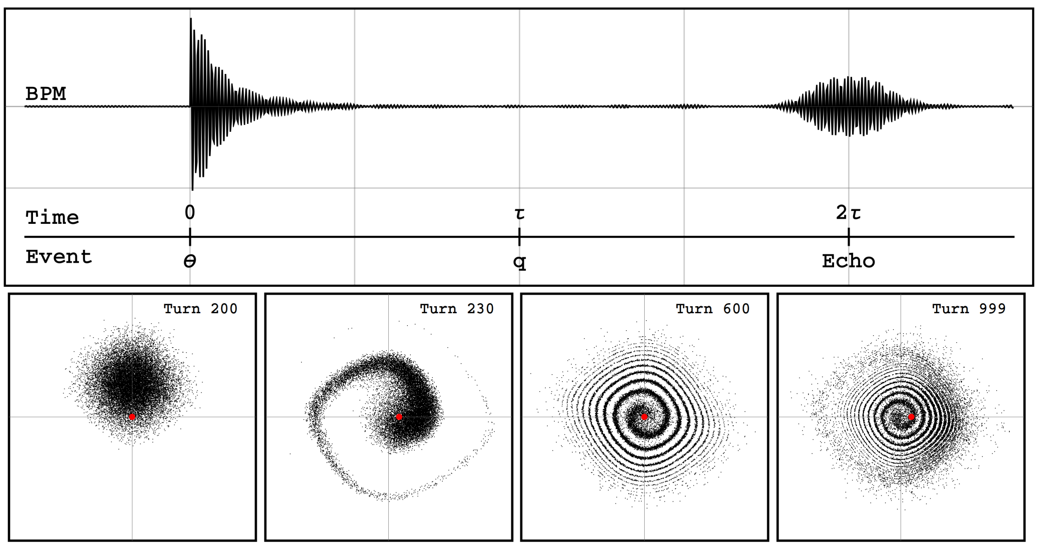

Figure 1: *Top:* Simulated BPM output for a typical echo sequence. *Bottom:* Phase space portraits a) after dipole kick, b) experiencing phase decoherence, c) after quad kick and d) at time of maximum echo amplitude. Red dot indicates beam position centroid.

Now, we apply a one-turn dipole kick θ at time $t = 0$. This is the second ingredient of the echo. The beam centroid is displaced from equilibrium and undergoes oscillation. However, due to phase decoherence, the centroid oscillation dies down with a characteristic time τ_{dec}.

The final ingredient in a basic echo comes long after the centroid signal has damped to zero (typically in hundreds of turns). At time $t = \tau$, we apply a one-turn quadrupole kick q to the beam. Interestingly, this causes the particles to recohere in phase, such that near time $t = 2\tau$, the relative phases of the particles begin to realign as they arrive back to their "original positions" in phase space. The phase recoherence effect results in centroid oscillation long after the initial dipole kick, thus giving rise to the eponymous "echo" signal. The effect of the quad kick can be thought of as to recover some of the original phase information present right after the dipole kick. An animation of the whole echo sequence can be found at Ref. 7.

2.2 Characteristics of an echo

If we assume an initial Gaussian beam distribution and linear action-dependence in ω, i.e.

$$\psi_0(J) = \frac{1}{2\pi J_0} e^{-J/J_0}, \tag{4}$$

$$\omega(J) = \omega_0 + \omega' J, \tag{5}$$

where J_0 is the initial emittance, ω_0 is the base betatron frequency and ω' is the detuning parameter, then we can solve for the echo amplitude analytically [3, 4]

$$\langle x \rangle_{\text{ampl}} (\Xi) = \frac{a_0}{(1+\Xi^2)^{3/2}}, \quad \text{where} \quad a = \theta q \sqrt{\beta\beta_k} \omega' J_0 \tau. \tag{6}$$

Here, a is the maximum amplitude of the echo, $\Xi \equiv \omega' J_0 (t - 2\tau)$ is the normalized time variable and β, β_k are the betatron functions at the BPM and dipole kicker respectively. It is also useful to define the normalized maximum echo amplitude:

$$A = \frac{a}{\sqrt{\beta\beta_k}\theta}. \tag{7}$$

We expect A to have a theoretical limit of 1, since we do not expect to recover more phase information in the echo than was present right after the dipole kick. In practice, saturation effects set in much sooner, as we shall see shortly. It is also important to note that we made two key assumptions in the analysis:

1. The delay time τ is much larger than the decoherence time τ_{decoh}.
2. Both dipole kick θ and quad kick q are weak.

These assumptions impose limits on our working parameter space. A precise mathematical statement of these assumptions can be found in Ref. 4.

2.3 Diffusion

Due to the influence of space charge and other intensity dependent effects, diffusion-like behavior is induced in the beam distribution. Over time, intra-beam scattering and nonlinear dynamics effects will cause a detrimental growth in emittance, which can become significant in high intensity beams. Mathematically, beam diffusion is modelled by the eponymous partial differential equation

$$\frac{\partial \psi}{\partial t} = \frac{\partial}{\partial J}\left(D(J) \frac{\partial \psi}{\partial J} \right), \quad \text{where} \quad D(J) = D_0 + \sum_n D_n \left(\frac{J}{J_0} \right)^n, \ n \geq 0. \tag{8}$$

Here, $\psi(J, \phi, t)$ is the beam distribution in phase space. The diffusion coefficient $D(J)$ can contain any number of linear or nonlinear terms. We will assume in this analysis that $n = 1$ (linear) for simplicity, i.e.

$$D(J) = D_0 + D_1 \left(\frac{J}{J_0} \right). \tag{9}$$

The maximum echo amplitude becomes attenuated with diffusion,

$$a_{\text{difn}} = a_0 \left(\frac{\exp(1-\alpha_0)}{\alpha_1^3} \right), \quad \text{where} \quad \alpha_i = 1 + \frac{2}{3} D_i \omega'^2 \tau^3. \tag{10}$$

The base amplitude a_0 is reduced by the multiplicative factor in parentheses. Both the exponential dependence on D_0 and inverse cubic dependence on D_1 highlight the particular sensitivity of the echo amplitude to diffusion. The new echo amplitude a_{difn} can also be maximized with respect to delay time τ and detuning ω'. Assuming D_0 is negligible, we find [6],

$$\tau_{\text{max}} = \left(\frac{16}{3} \omega'^2 D_1 \right)^{-1/3}, \tag{11}$$

$$\omega'_{\text{max}} = \left(\frac{10}{3} \tau^3 D_1 \right)^{-1/2}. \tag{12}$$

Qualitatively, τ_{max} and ω'_{max} represent the respective "optimal" parameter value where echo amplitude is at a maximum. These relationships will prove useful for measuring the diffusion coefficient D_1 if we can ascertain the value of τ_{max} or ω'_{max} via a series of echo measurements.

2.4 Pulsed Quadrupoles

It is possible for strong diffusion (e.g. arising from space charge) to completely attenuate the echo signal. Thus, we require techniques to boost echo amplitude. Pulsed quadrupoles is one such method.

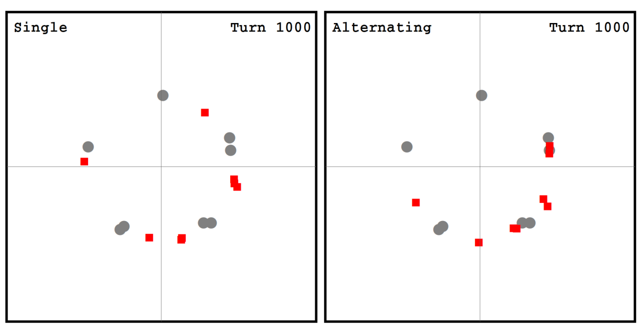

Figure 2: Phase space portraits of a small subset of the beam particles at time of echo. Grey particles received no quad kick, while red particles received either a single quad kick (left) or an alternating series of kicks (right). Note that the red particles on the right are more tightly grouped, thus resulting in a stronger echo signal.

A pulsed quadrupole sequence extends the single quad kick at τ into a pattern of kicks. Each subsequent quad kick is timed in order to reinforce the effect of the preceeding kick. At 2τ, a tighter grouping of particles in phase space would be formed, thus producing a stronger echo signal (Fig. 2). We experimented with various kick sequences, as well as the length of the pulse sequence (in number of additional kicks). Finally, we also examined the possibility for amplification of multi-echo sequences.

Notation wise, we use character sequences such as 'pnpn' to describe the pulsed quadrupoles. One turn positive kicks were indicated with 'p', while 'n' denoted similar negative kicks. The absence of a kick for one turn would be marked with 'x'. Furthermore, the length of the sequence N_{pulse} is measured in terms of the number of *additional* kicks. Therefore, the sequence 'pnpn' has length 3 and indicates a positive kick at τ turns, negative kick at $\tau + 1$, positive kick at $\tau + 2$, and finally negative kick at $\tau + 3$.

For alternating 'pn' sequences, the beam centroid can be found by numerical integration [6] of

$$\langle x \rangle_n = -\frac{\pi\beta\theta q\tau\omega'}{J_0^2} \int_0^\infty dJ\, J^2 e^{-J/J_0} \left(\frac{\sin\omega(J)(t-2\tau+\tau_0) + (-1)^n \sin\omega(J)(t-2\tau-(2n+1)\tau_0)}{\cos\omega(J)\tau_0} \right), \quad (13)$$

whence we can obtain a prediction for maximum echo amplitude. Here, $n = N_{\text{pulse}}$ and τ_0 is the delay time between each successive kick (typically the revolution time).

3 Simulation

The simulation used in this study was written from scratch in C. The program tracked the phase space Floquet coordinates of individual beam particles and propagated them along a simulated storage ring (based on RHIC machine parameters [5]) over a preset number of turns. Typical parameters of the simulation are listed in Fig. 3. Subsequent data analysis and visualization were performed with *Mathematica*.

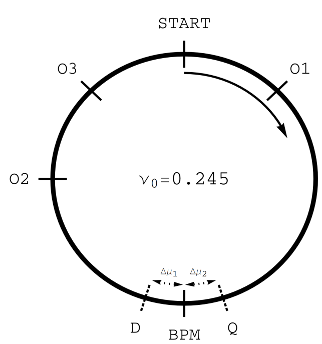

Parameter	Symbol	Value
Number of particles	N_{part}	20000 to 50000
Unnorm. rms emittance [m-rad]	ϵ_0	1.5×10^{-7}
Rms beam size [m]	σ_x	3×10^{-3}
Transverse tune	ν_0	0.245
Betatron at BPM, dipole and quad [m]	β, β_k, β_q	10, 10, 10
Detuning	μ	10^{-4} to 10^{-3}
Dipole kick [rad]	θ	10^{-4} to 10^{-3}
Norm. quad strength	q	0.01 to 0.05
Timing of quad kick [turns]	τ (or τ_q)	400 to 1000

Figure 3: *Left:* Schematic of simulated ring based on RHIC parameters [5]. Dipole, quadrupole and octupoles are labelled with 'D', 'Q' and 'O' respectively. *Right:* Typical values used in simulation.

We typically begin with a Gaussian beam distribution (although various other uniform distributions were also studied). The octupole magnets provided the linear detuning $\omega(J)$. Diffusion, if present, was implemented as Gaussian dipole noise applied at the end of each turn.

In general, simulation results displayed good consistency with theory (Fig. 4). We observed significant discrepancy at high values of q, θ and ω', which can be attributed to the breakdown of the aforementioned theory assumptions. Furthermore, saturation was also observed at normalized echo amplitude $A \approx 0.4$.

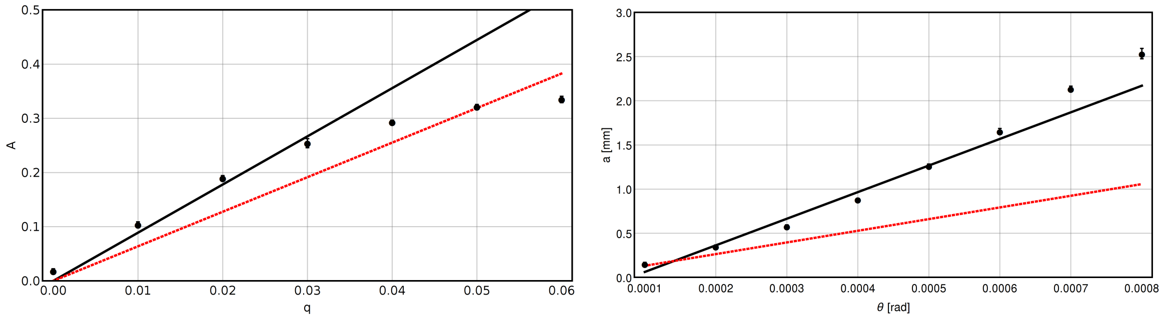

Figure 4: Plots of normalized echo amplitude versus quad strength (left), echo amplitude versus dipole kick (right) and emittance increase versus dipole kick (inset). At low values, there is good agreement between simulation (black) and theory (red). Significant discrepancy is apparent for larger parameter values. Furthermore, saturation is observed to set in for high q as normalized amplitude A approaches 0.4.

4 Results

4.1 Diffusion measurement

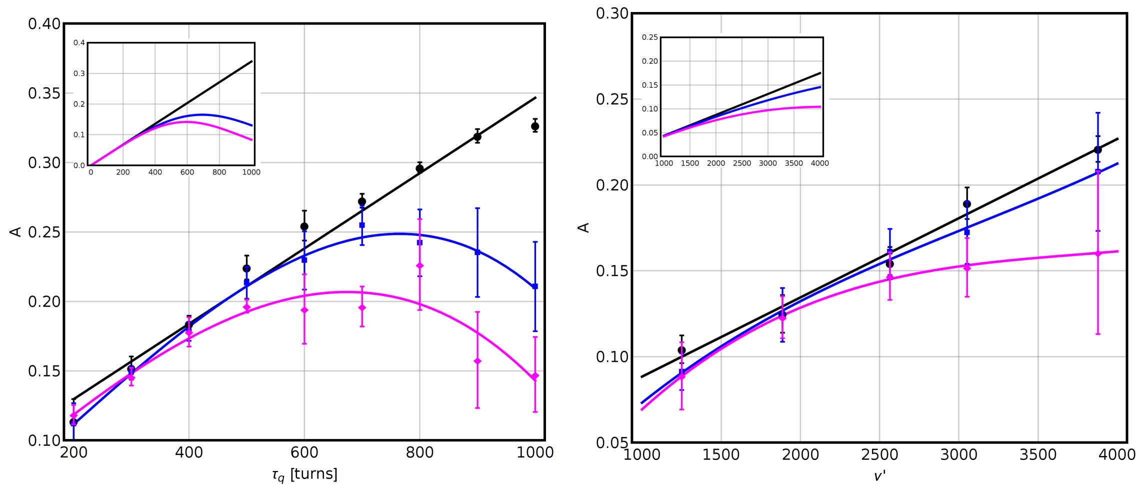

Figure 5: Plots of normalized echo amplitude versus delay time (left) and detuning parameter (right). Note that $\nu' = \frac{\omega'}{\Omega}$, where Ω is the revolution frequency. Simulation results are in good agreement with theory (insets).

Simulation results from parameter scans over τ and ω' displayed the expected theoretical relationships with echo amplitude (Fig. 5). Furthermore, by estimating τ_{max} we were able to use equation 10 to determine the linear diffusion coefficient D_1.

For Gaussian dipole noise of magnitude $\theta_R = 1 \times 10^{-6}$ rad, we calculated $D_1 = 1.5 \times 10^{-18}$ m-rad^2/turn using this method. This was corroborated against a straightforward measurement of D_1 by tracking emittance growth over time (Fig. 6):

$$D_1 = \pi\epsilon_0 \frac{\mathrm{d}\epsilon}{\mathrm{d}t}, \tag{14}$$

where ϵ_0 is the intial emittance. We obtained $D_1 = 1.4\times10^{-18}$ m-rad^2/turn, which is in excellent agreement with our previous estimate. This demonstrates self-consistent results from the simulation.

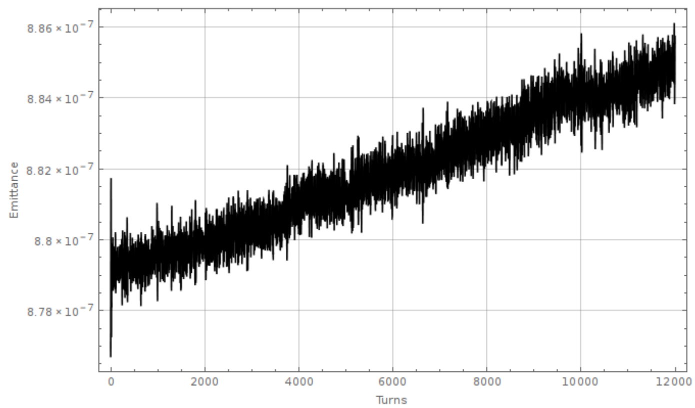

Figure 6: Linear increase in emittance over time due to Gaussian dipole noise. We were able to confirm the diffusion coefficient D_1 by tracking rate of emittance increase.

4.2 Pulsed quadrupoles

Our findings with regards to pulsed quadrupoles can be summarized into four main points.

1. Pulsed quadrupoles are an effective means to boost echo amplitude, with a caveat. We investigated echo amplitude versus kick length using both alternating ('pn') and single-polarity ('pxpx') sequences (Fig. 7). Starting with an unboosted amplitude of $A = 0.18$, we achieved maximum amplification of almost 100%. This clearly demonstrates the effectiveness of using pulsed quadrupoles to boost echo amplitude. The caveat is that echo amplitude is still subject to saturation at $A \approx 0.4$. We were unable to surpass this empirical limit regardless of kick strength, length or pattern.

2. Optimum pulse sequence is highly dependent on fractional tune. Due to the intricate interplay between the timing of the pulse kicks and the phase advance of the particles, we observed the transverse fractional tune to be a significant factor in choosing the optimum pulse sequence. For fractional tunes close to $1/4$ or $3/4$, we found the alternating sequence ('pn') or single polarity alternating sequence ('px') to be most effective (Fig. 7). For tunes close to integer values or $1/2$, the repeating sequence ('pp') was more appropriate. In fact, if an inappropriate sequence was used for the particular tune (e.g. the 'pp' sequence for fractional tune close to $1/4$), it is possible to suppress or completely destroy the echo signal.

3. Alternating quadrupoles are optional. An alternating quadrupole of sufficiently high frequency is a significant challenge to build with current magnet technology. Fortunately, the alternating kick sequence 'pn' can be effectively replaced with the single polarity quadrupole sequence 'pxpx'. In our study of echo

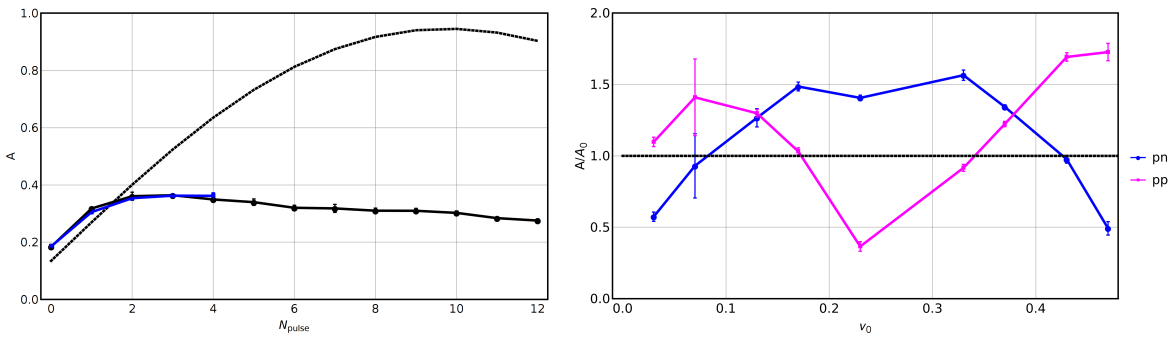

Figure 7: *Left:* Normalized echo amplitude versus kick length. Saturation sets in after $N_{\text{pulse}} = 2$ with $A \approx 0.4$. We tested both alternating sequence (black) and the equivalent single polarity sequence (blue), with minimal difference between the two. Theory (black, dotted) was obtained using numerical solution of equation 13. *Right:* Fractional increase in amplitude versus machine tune. Alternating sequence is favored by tunes close to $1/4$ (or $3/4$) while repeated sequence is better for tunes close to integer values or $1/2$.

amplitude versus kick length (Fig. 7), we also compared the performance of the 'pxpx' sequence to the 'pn' sequence and found them to be effectively identical up to saturation.

In each case, the equivalent 'pxpx' sequence was determined by replacing all negative kicks with no kick, and doubling the length of the sequence to conserve the overall number of kicks. For example, the equivalent sequence to 'pnpn' would be 'pxpxpxpx'. This substitution rule works only for tunes close to $1/4$ or $3/4$. However, we expect similar single-polarity sequences to exist for any fractional tune close to a m/n fraction for m, n integers (e.g. the sequence 'pxxpxx' for tune $1/3$, sequence 'pxxxxpxxxx' for tune $1/5$ and so on).

4. Multi-echo amplification is also possible. In addition to the 2τ echo, we expect to observe echoes at 4τ, 6τ etc. even with a single quadrupole kick (Fig. 8). However, the amplitudes of these secondary echoes are usually much weaker and thus difficult to measure. In simulation, we found that it is possible to boost the amplitude of the secondary echoes by applying additional quadrupole kicks at multiples of τ. For example, if we apply kicks at τ and 2τ, we observe a much stronger 4τ echo. If we apply kicks at every multiple of τ, we find the resulting multi-echo sequence to be stable in amplitude. Interestingly, if diffusion is then added, the multi-echo max amplitudes decrease over time.

Multi-echo amplification can be explained, though not completely, by the superposition of echoes [4]. If we apply kicks at τ and 2τ, we expect the 4τ echo to be much stronger due to the superposition of the second echo in the τ-sequence and first echo in the 2τ-sequence. This is supported by simulation results. However, we also observed amplification of the 6τ echo (Fig. 8), which cannot be thusly explained since the 2τ-sequence does not give rise to an echo at 6τ.

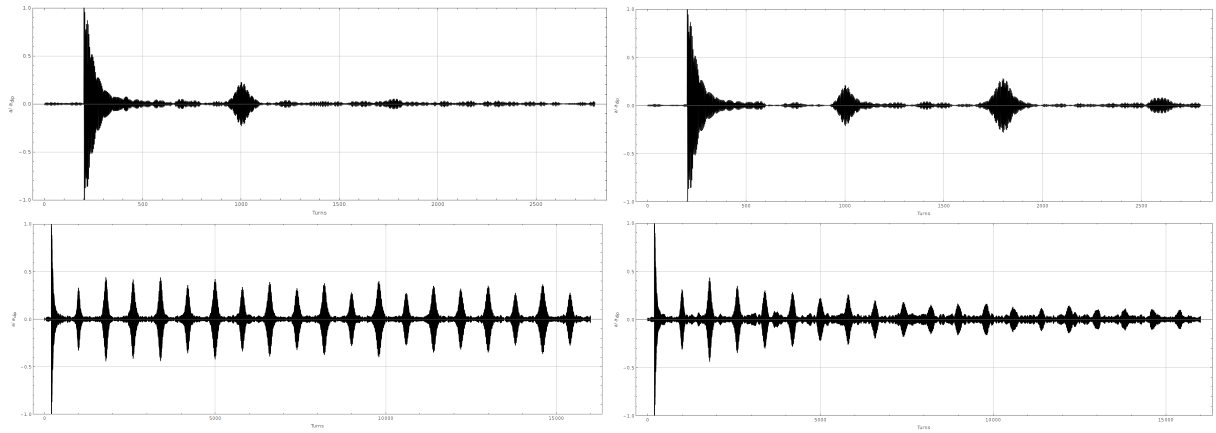

Figure 8: *Left to right, from top:* a) Single quad kick giving rise to echoes at 2τ and 4τ. The 6τ echo is not visible. b) Quad kick applied at τ and 2τ. We observe amplification of the 4τ echo and, curiously, also the 6τ echo. c) By applying quad kicks at every multiple of τ, we achieved a stable echo sequence. d) When diffusion was added, the echo sequence displayed decreasing max amplitudes with time.

5 Conclusion and Discussion

To recap the main findings of this study:

1. We were able to perform a self-consistent measurement of the D_1 linear diffusion coefficient using a parameter scan over delay time τ.
2. Pulsed quadrupoles are an effective means to boost echo amplitude, up to the saturation point.
3. The optimum pulse sequence is highly dependent on the fractional tune of the machine.
4. Alternating pulse sequences are optional — one can always replace them with equivalent single-polarity kick sequences.
5. Multi-echo amplification is possible through quadrupole kicks applied at multiples of τ.

For future studies, we recommend the following unresolved areas for investigation.

Saturation is one of the main barriers to further amplification of the echo signal. Theoretically, saturation arises in the limit where the assumptions of weak q and θ break down. Currently, we do not have an accurate theoretical model accounting for saturation. Empirically, we observed saturation to occur near normalized echo amplitude $A \approx 0.4$. Past that point, the singly-peaked echo signal was observed to broaden and eventually split into a weaker doubly-peaked signal (Fig. 9).

Curiously, the saturation limit is independent of the method used to boost the echo. For single quadrupole kicks, saturation was observed when increasing the parameters τ, q, ω'. For pulsed quadrupoles, simply increasing the number of kicks was enough induce saturation. In all cases, the saturation limit was $A \approx 0.4$. Could this limit prove to be the full extent of recoverable phase information, or is there a way to overcome this barrier?

Due to time constraints, we were able to test only a small subset of possible pulse sequences. In partic-

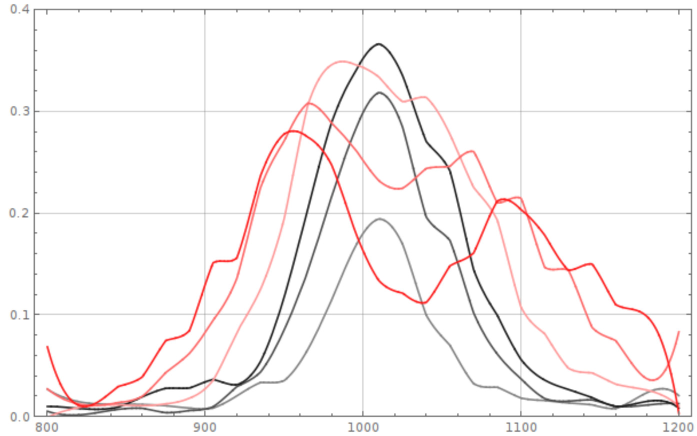

Figure 9: Envelopes of various echo signals. Before saturation, the echo signal grows in both height and width (increasing shades of black). Past saturation, the echo signal ceases to grow in amplitude, but instead broadens and splits into two peaks (increasing shades of red).

ular, multi-echo amplification still holds many unanswered questions which warrant further study. Also, we hope to extend the simulation program to the full two dimensional transverse plane. This would allow us to study the effects of coupling on echoes in both the x and y planes, as well as any other higher order phenomena. Finally, we would also like to include IOTA-specific parameters in preparation for the planned echo measurement experiment.

This research project was made possible by the Lee Teng Fellowship in Accelerator Science and Engineering hosted by Fermilab. Additionally, the author would like to thank his research mentor Dr. Tanaji Sen, internship director Dr. Eric Prebys, and the knowledgeable instructors at USPAS for their invaluable guidance and support.

6 References

1. HEPAP P5 Interactive Report, June 2014, pp. 12.
2. G. Valentino *et al.*, *Phys. Rev. ST Accel. Beams* **16**, 021003 (2013).
3. G. Stupakov, Report No. SSCL-579, (1992).
4. A. Chao, *Echoes*, SLAC National Accelerator Laboratory, Lecture Notes.
5. W. Fischer, T. Satogata and R. Tomas, in *Proceedings of PAC'05, Knoxville, Tennesse* (IEEE, New York, 2005), pp. 1955-1957.
6. T. Sen, *Echoes Notes*, Fermilab TM (to be published).
7. An animation created by this author can be found at `https://youtu.be/l54tM4MBEVI`.